Desalination and Water Treatment
www.deswater.com
doi: 10.5004/dwt.2021.26553

210 (2021) 351–364
January

One-pot synthesis of nano-$MnFe_2O_4$ decorated Al_2O_3 and its application in Cu^{2+} adsorption

Zhanmeng Liu[a,b,*], Gang Chen[b], Xian Li[b], Xiuguo Lu[b]

[a]*School of Civil Engineering and Architecture, Nanchang Institute of Technology, Nanchang 330099, China, Tel. 86-791-87046054; Fax: 86-791-87046027; email: ustblzm@sina.com (Z. Liu)*
[b]*School of Civil Engineering and Architecture, East China Jiao Tong University, Nanchang 330013, China, emails: cglj930726@sina.com (G. Chen), ecjtu@126.com (X. Li), xiuluolu@sina.com (X. Lu)*

Received 11 April 2020; Accepted 6 September 2020

ABSTRACT

Through coating the magnetic nano-$MnFe_2O_4$ onto the surface of Al_2O_3, a kind of magnetic composite of nano-$MnFe_2O_4/Al_2O_3$ adsorbent was synthesized successfully and used for the copper ions removal from simulated wastewater. The composite was characterised using a vibrating sample magnetometer, scanning electron microscopy, X-ray powder diffraction, Fourier transform infrared spectroscopy, X-ray photoelectron spectroscopy, and a Brunauer–Emmett–Teller analysis. At the same time, the response surface method was used to optimize the reaction parameters. Moreover, the studies of adsorption isotherms and kinetics indicated that the Cu^{2+} adsorption process may be a multilayer chemical adsorption. It was worth noting that the increased concentration of F^- favored the Cu^{2+} adsorption. Under the optimum conditions, when the initial concentration of Cu^{2+} was 20 mg/L and the adsorbent dosage was 0.20 g, the removal rate was 98.2%. In addition, after five cycles, the removal rate dropped only from 98.2% to 85.7%. This prepared magnetic adsorbent possessed excellent adsorption property and the characteristics of great reusability with quick solid-liquid separation from aqueous solution under external magnetic field added, which indicated its potential practical application for the Cu^{2+} removal from wastewater.

Keywords: Adsorption; Solid–liquid separation; Heavy metals; Response surface method; Reusability

1. Introduction

With the rapid industrialization of human society, the environmental problems caused by the emission of pollutants have attracted more and more attention from researchers in the field of environment [1,2]. The component of contaminated wastewater varies very much according to its source, but the typical contaminations are dyes, phenolic and anilinic compounds, surfactants, heavy metals, antibiotics, and other aerobic substances [3–5]. However, the contamination due to heavy metals, which are derived from mining, battery industry, metal processing, and machinery manufacturing, is a focus of worldwide environmental problem due to its persistent toxicity and nonbiodegradability in the environment [6]. Furthermore, heavy metals are prone to accumulate in the living organisms, and may lead to irreversible diseases, such as cancer, central nervous and brain damage, etc. [7].

Copper, the most widely and first used heavy metals, has been reported to be used to manufacture weapons and multifarious implements as well as other utensils in the

* Corresponding author.

prehistoric age, which reached its applied heyday in the Shang Dynasty in China. Nowadays, owing to the excellent electrical conductivity of copper, it is more preferred to be used in the electrical industry [8]. For human body, copper element plays a vital role in the processing of metalloenzymes such as cytochrome oxidase, superoxide dismutase, and tyrosinase [9]. Nevertheless, excessive intake of food easily accumulated with copper, such as liver, shellfish, mushrooms, nuts, and chocolate, as well as long-term exposure to the drinking water contained copper even at trace level, would cause neurotoxicity, jaundice, and liver toxicity [10]. Accordingly, removal of copper from water with a cost-effective and efficient method should be considered as an urgent issue, which is to be solved.

The application of adsorption for the removal of heavy metals has received considerable attention all the time. Comparing with other techniques, such as solvent extraction separation [11], membrane [12], chemical precipitation [13], ion exchange [14], electrochemistry [15], microbial biotechnology [16], adsorption is the most widely applied one for the removal of heavy metals due to its lower operation cost, higher selectivity, greater recovery efficiency, and less secondary pollution [17]. At the same time, the process of finding adsorbents with high efficiency and large adsorption capacity of target heavy metals is pursued by the researchers in this field. Although activated carbon alone was usually covered as an independent adsorbent for the removal of heavy metals and/or dyes due to its large specific surface area and adsorption capacity, its low settlement performance and residual materials in supernatant even with high speed centrifugation limited their usage in some situations.

Recently, with the conceptions of environmental protection and sustainable development deep in people's heart, magnet-based adsorbents were favored by more and more researchers as a result of its quick and easy separation from aqueous solution with an external magnetic field added. Manganese ferrite ($MnFe_2O_4$), a spinel material, of which structure like Fe_3O_4, has been reported as a promising adsorbent for heavy metal ions from aqueous solution due to its high specific surface area [18]. However, the efficiencies of using nano-$MnFe_2O_4$ alone for the Cu^{2+} ions removal revealed in this experiment were relatively low and the solutions after treated did not satisfy the standards of wastewater discharge, which indicated that the adsorbents synthesized should be further modified. The commonly applied modifications include treating adsorbents with acid, alkali, surfactant, loading, and so on, of which the modifying mechanism either enlarges the specific surface area or increases the functional groups that easily get complexed with adsorbate, or is a combination of two mechanisms [18,19]. Among the modifying methods, loading modification is more controllable and the goal of modification is easy to achieve. Hence, to enlarge the specific surface area and adsorption capacity of $MnFe_2O_4$, it is necessary to find a loading material with larger specific surface area.

Alumina is an amphoteric metal oxide with good thermal stability, large surface area, and remarkable adsorption capacity [20]. This has been also reported as an adsorbent for the removal of fluoride [21], dyes [20], and heavy metals [22]. However, it is hard to separate alumina quickly from the aqueous solution after the adsorption process. Recently, contributing to the inherited characters of composited adsorbents from raw materials comparing with the simplex adsorbents, researchers preferred to turn their direction towards the research of alumina-based adsorbents. Wei et al. [23] synthesized a novel CNTs/Al_2O_3 adsorbent for the removal of diclofenac sodium and carbamazepine, and the maximum sorption capacities reached 157.4 and 106.5 μmol/g, respectively. And they found that after 10 regeneration experiments, CNTs/Al_2O_3 still maintained good stability, and the removal rate of carbamazepine was only reduced by about 10%. Sun et al. [24] prepared Fe_3O_4/Al_2O_3 nanoparticles for the analysis of sulfonamides in different soil samples, which can not only achieve good recoveries of sulfonamides but also reduce the analysis time with magnetic solid-phase extraction. However, hitherto there are few reports about $MnFe_2O_4/Al_2O_3$ as adsorbent for the removal of heavy metal ions from aqueous solution.

The objective of this paper is to illustrate the good adsorption capacity of $MnFe_2O_4/Al_2O_3$ for Cu^{2+} removal and find out the optimal operating conditions. Accordingly, in this study, as-prepared magnetic adsorbents, $MnFe_2O_4/Al_2O_3$ nanoparticles were obtained from manganese ferrite loading onto the surface of alumina via dipping method and they were applied for the investigation of copper ions adsorption performance. The physicochemical properties of obtained nano-$MnFe_2O_4$ and nano-$MnFe_2O_4/Al_2O_3$ were characterized in detail. The effects of pH, adsorbent dosage, initial adsorption concentration, and reaction time on the removal of Cu^{2+} were investigated. In addition, the response surface method (RSM) was used to optimize the reaction parameters. Furthermore, the regeneration performance of the prepared adsorbent was investigated, and the results showed that the adsorption capacity of the prepared adsorbent only decreased from 9.82 to 8.57 mg/g after five cycles of regeneration experiments. These results indicated that the prepared nano-$MnFe_2O_4/Al_2O_3$ has promising application for Cu^{2+} removal in wastewater.

2. Materials and methods

2.1. Materials and reagents

Copper sulfate pentahydrate ($CuSO_4{\cdot}5H_2O$), sulfuric acid (H_2SO_4), sodium hydroxide (NaOH), absolute ethyl alcohol (CH_3CH_2OH) and ethanediol $(CH_2OH)_2$ were purchased from Xilong Scientific Co., Ltd. (Shantou, Guangdong, China) and they are all GR reagents. Ferric nitrate ($Fe(NO_3)_3{\cdot}9H_2O$, AR) was obtained from Tianjin Hengxing Chemical Reagent Manufacturing Co., Ltd. (China). Potassium permanganate ($KMnO_4$, AR) was purchased from the Shanghai Chemical Technology Company (China). Aluminium oxide (Al_2O_3, AR) was received from Tianjin Damao Chemical Reagent Factory (China). Ammonium acetate (NH_4Ac, AR) was supplied by Shanghai Zhanyun Chemical Co., Ltd. (China). Polyethylene glycol (PEG 4000, AR) was provided by Tianjin Comiao Chemical Reagent Co., Ltd. (China). The stock solutions of F^-, Cl^-, NO_3^-, and SO_4^{2-} were purchased from Beijing TanMo Quality Inspection Technology Co., Ltd. (China). Ultrapure water (18.25 MΩ, UPC-III-20T, China) was used to prepare multifarious solutions throughout the experiments.

2.2. Preparation and characterization of nano-$MnFe_2O_4/Al_2O_3$

The preparation of nano-$MnFe_2O_4/Al_2O_3$ can be divided into two steps. First, 4.04 g of $Fe(NO_3)_3{\cdot}9H_2O$ and 0.79015 g of $KMnO_4$, whose molar ratio was 2:1 of Fe^{3+}:Mn^{2+}, was mixed in 80 mL of ethanediol by stirring at 60°C and 3,000 rpm with a magnetic stirrer (model DF-101S, Gongyi City Yuhua Instrument Co., Ltd., China). Then, 3.854 g NH_4Ac was added slowly to keep the pH of the solution neutral, and 3.0 g PEG 4000 was applied as a structural guidance agent. After adequate stirring, the resultant yellowish mixture was placed into a 100 mL of PTFE lined reactor and sealed to heat at 180°C for 12 h in an electric blast drying oven (model WGL-125B, Tianjin Taisite Instrument Co., Ltd., China). The obtained precipitates were washed repeatedly with ethanol and ultrapure water several times after separated with magnet. After that, the solid was dried at 80°C for 6 h in a vacuum drying oven (model Shanghai Kuntian Laboratory Instrument Co., Ltd., China). The prepared powder through these procedures was characterized as nano-$MnFe_2O_4$. The composites of nano-$MnFe_2O_4$/Al_2O_3 were synthesized by the dipping method. 6.0 g Al_2O_3 pre-treated by cleaning and drying and 1 g prepared nano-$MnFe_2O_4$ through the method above were weighed and placed in a 250 mL triangular conical bottle filled with 100 mL ultrapure water. Afterwards, the mixture was subjected to ultrasonic oscillation (model KQ5200DE, Kunshan Ultrasonic Instrument Co., Ltd., China) for 30 min, and placed in a water bath constant temperature oscillator (model SHZ-82, Changzhou Guohua Electric Appliance Co., Ltd.) for dipping 12 h at 30°C with rotation rate of 200 rpm. The obtained precipitates were washed repeatedly with ethanol and ultrapure water several times and separated with magnet and dried at 80°C for 6 h to apply for further series of adsorption experiments.

Vibrating sample magnetometer (VSM, model PPMS–9T, Quantum Design North America, USA) was used to analyze the magnetic properties of the nano-$MnFe_2O_4/Al_2O_3$ and the saturation magnetization was measured from the hysteresis curve. Zeta potential analyzer (model ELSZ-2000, Otsuka Electronics Co., Ltd., Japan) was used to analyze zeta potential of solution. The morphology and microstructure of the nano-$MnFe_2O_4/Al_2O_3$ was observed with field emission scanning electron microscopy (SEM, model JSM-7100F, Japan Electronics Co., Ltd., Japan) with an accelerating voltage of 30 kV. The powder X-ray diffraction (XRD) patterns of nano-$MnFe_2O_4/Al_2O_3$ were recorded on an X'Pert PRO diffractometer (PANalytical B.V., Netherlands) with an Ni-filtered Cu Kα radiation (λ = 0.15416 nm) in the range of 2θ = 5°–90° at the operating conditions of 40 kV and 40 mA. The specific surface area and pore size were measured following the Brunauer–Emmett–Teller (BET) method using a specific surface area analyser (Nova 2000e, Quantachrome Instruments, USA). The Fourier transform infrared (FTIR) spectroscopy measurements were performed by a spectrometer of Nicolet 6700 (Thermo Fisher Scientific Co., Ltd., USA) at the best resolution of 0.5 cm^{-1} over the total range of 8,000–50 cm^{-1}. X-ray photoelectron spectroscopy (XPS) was carried out on a multifunctional high performance surface analyzer (model Escalab 250Xi, Thermo Fisher Scientific Co., Ltd., USA) at constant pass energy of 30.0 eV and energy step size of 0.10 eV, of which the X-ray source is Al Kα radiation (hν = 1,486.6 eV).

2.3. RSM experiments

The standard stock solution of concentration 1,000 mg/L Cu^{2+} was prepared with 3.9720 g $CuSO_4{\cdot}5H_2O$ settled in constant volume in 1,000 mL volumetric flask by ultrapure water. The various Cu^{2+} concentrations used in subsequent experiments were all diluted with this stock solution.

Batch experiments were conducted in a 250 mL conical flask containing 100 mL of Cu^{2+} solution. The solutions of 0.1 M H_2SO_4 and NaOH were employed for the adjustment of the solution pH before each experiment, and the pH values were measured by pH meter (model SJ-3F, Shanghai Shengke Instrument Equipment Co., Ltd., China). The Cu^{2+} concentration was determined using an atomic absorption spectrometer (AAS, model PinAAcle 900T, PerkinElmer Enterprise Management [Shanghai] Co., Ltd., China).

According to the Box–Behnken [25] design scheme, a set of 17 experiments with 3 factors and 3 levels was designed (all the experimental water samples were simulated water samples containing Cu^{2+} 20 mg/L). The experimental factors, levels and codes are shown in Table 1.

The following equations (Eqs. (1) and (2)) can be used to determine the amount of Cu^{2+} adsorbed on the nano-$MnFe_2O_4/Al_2O_3$,

$$R(\%) = \frac{(C_0 - C_e)}{C_0} \times 100\% \tag{1}$$

$$Q_e = \frac{(C_0 - C_e)}{m} \times V \tag{2}$$

where R(%) represents the removal efficiency and Q_e indicates the adsorption capacity (mg/g) of Cu^{2+} ions at adsorption equilibrium; C_0 is the initial concentration metal ion (mg/L) and C_e is the residual concentration of adsorbate (mg/L) in the solution at adsorption equilibrium; V is the volume of Cu^{2+} solution (L), while m is the mass of adsorbent (g), respectively.

2.4. Adsorption kinetics and isotherms studies

2.4.1. Adsorption kinetics

In this part, 100 mL of 20 mg/L Cu^{2+} solution was first added in a 250 mL conical flask. Subsequently, adjusting the pH value to 6.0, adding 0.20 g nano-$MnFe_2O_4/Al_2O_3$

Table 1
Box–Behnken experimental factors, coding and levels

Factors	Levels and codes		
	–1	0	1
pH	3.0	4.5	6.0
Dosage (g)	0.1	0.2	0.3
Reaction time (h)	2.0	3.0	4.0

as adsorbent, the experiment was conducted under the conditions at 4 h reaction time, 30°C and 230 rpm. Every 30 min, 5 mL solution of supernatant was taken out into 50 mL comparison tubes for dilution and then the residual Cu^{2+} concentration in solution was examined with AAS.

Adsorption kinetics is essential to analyze the adsorption mechanism and interpret the adsorbate uptake rate. In order to describe the relationship between the adsorbate uptake rate and reaction time, the models of pseudo-first-order and pseudo-second-order were applied for acquisition of various kinetic parameters in this study. The equations of adsorption kinetics were expressed as following (Eqs. (3) and (4)) [26]:

Pseudo-first-order:

$$\ln\left(q_e - q_t\right) = \ln q_e - k_1 t \tag{3}$$

Pseudo-second-order:

$$\frac{t}{q_t} = \frac{1}{k_2 q_e^2} + \frac{t}{q_e} \tag{4}$$

where q_t is the adsorption capacity (mg/g) at time t (min). k_1 (1/min) and k_2 (g/mg min) are the pseudo-first-order and pseudo-second-order adsorption rate constant, respectively.

2.4.2. Adsorption isotherms

In this study, 5, 10, 15, 20, 30, 40, 50 mg/L Cu^{2+} were chosen for adsorption onto 0.20 g nano-$MnFe_2O_4/Al_2O_3$, and this experiment was conducted with all parameters at optimal range (pH 6.0, 4 h reaction time, 30°C and 230 rpm). Models of Langmuir and Freundlich adsorption isotherms were selected to provide insights about the surface properties and affinity of the adsorbent as well as adsorption mechanism [27].

Although there are many types of adsorption isotherm models, the Langmuir and Freundlich adsorption isotherm models are widely used to illustrate the relationship between the adsorption capacity and residual adsorbate concentration [28].

Langmuir adsorption isotherm implies that the process of adsorption is a simple physical adsorption based on monolayer, and its equation is as follows (Eq. (5)) [29],

$$\frac{C_e}{q_e} = \frac{1}{K_L q_m} + \frac{C_e}{q_m} \tag{5}$$

where q_e is the adsorption capacity (mg/g) at adsorption equilibrium, q_m is the maximum adsorption capacity (mg/g), and K_L (L/mg) is the Langmuir adsorption equilibrium constant. Generally speaking, the more the value of K_L, the stronger the adsorption property, of which, the value of K_L is related with the characteristic of adsorbent and adsorbate, and temperature.

Freundlich adsorption isotherm is used to describe multilayer and heterogeneous surface adsorption, and Eq. (6) can express this experimental model [30],

$$\ln q_e = \ln K_F + \frac{1}{n}\ln C_e \tag{6}$$

where K_F (mg/g) is the Freundlich constant and $1/n$ is an adsorption strength index which is related with heterogeneity of materials and its value varies from 0 to 1.

2.5. Desorption and regeneration study

The regeneration experiment was carried out under the conditions of initial concentration of Cu^{2+} = 20 mg/L, adsorbent dosage = 0.2 g, adsorbate volume = 100 mL, pH = 6.0, temperature = 30°C and shaking speed = 230 rpm. With regard to desorption experiment, the spent adsorbent was separated first from the aqueous solution with the aid of magnet. Subsequently, the collected adsorbent was mixed with 20 mL of 0.03 mol/L HNO_3 solution and shook for 2 h for adequate desorption. At last, the suspensions were filtered and the adsorbent was washed via ultrapure water several times. After drying, the reclaimed adsorbent was used for a new cycle of Cu^{2+} adsorption. With repeated desorption process, five consecutive cycles were carried out.

3. Results and discussion

3.1. Characterization of the adsorbents

3.1.1. Vibrating sample magnetometer

To examine the magnetic property and obtain the magnetic hysteresis loop of nano-$MnFe_2O_4/Al_2O_3$, the VSM instrument was employed, and the magnetization curve is presented in Fig. 1. It can be seen from the figure that the coercivity (H_c) and remanence (M_r) of nano-$MnFe_2O_4/Al_2O_3$ were almost negligible and close to 0, which presents superparamagnetism of nano-$MnFe_2O_4/Al_2O_3$. The saturation magnetism was 7.81 emu/g, which was sufficient to separate the adsorbents from the aqueous solution with an external magnetic field added. Actually, the aqueous solution containing nano-$MnFe_2O_4/Al_2O_3$ achieved its solid–liquid separation in about 2 min with the addition of permanent magnet, further identifying the great magnetic property of nano-$MnFe_2O_4/Al_2O_3$.

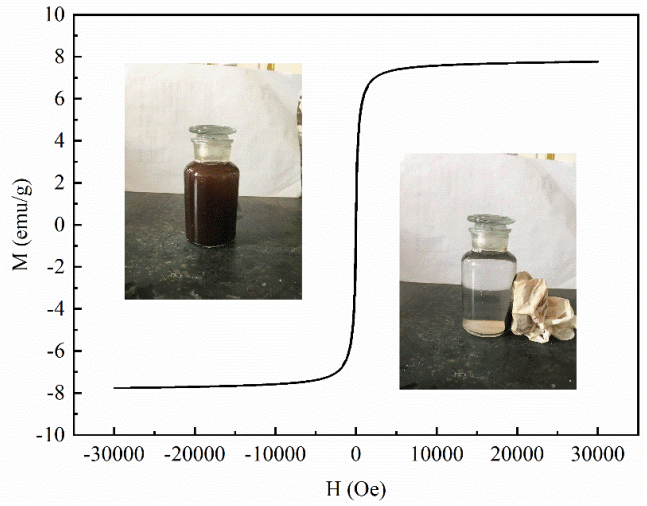

Fig. 1. Hysteresis loops and magnetic separation of nano-$MnFe_2O_4/Al_2O_3$.

3.1.2. SEM and TEM

To know the size, shape, and morphology of the adsorbent before and after modification with alumina, the SEM analyses were carried out. Figs. 2a and b present the micro-structural images of the nano-$MnFe_2O_4$ at 50,000 and 2,000 magnification times. As it can be seen, the nano-$MnFe_2O_4$ obtained with the method introduced in this article were regular spherical-like and the average particle size was approximately 80 nm. However, after the modification with Al_2O_3, either the particle size or morphology of the adsorbent changed a lot. Figs. 2c and d exhibit the micro-structural images of the nano-$MnFe_2O_4/Al_2O_3$ at 20,000 and 100 magnification times. It was obvious that the particle size of nano-$MnFe_2O_4/Al_2O_3$ increased greatly than that of nano-$MnFe_2O_4$ and the shape changed to more irregular. This could be ascribed to the large particle size and irregular shape of the Al_2O_3. Moreover, a cranny and something others different from Al_2O_3 could be observed on the surface of Al_2O_3 at 20,000 magnification times of nano-$MnFe_2O_4/Al_2O_3$. As can be seen from Fig. 2e, $MnFe_2O_4$ was relatively evenly distributed on the surface of Al_2O_3, and the average particle size of $MnFe_2O_4$ on the surface of Al_2O_3 was about 45 nm according to the calculation of relevant literature [31]. Combining the two figures of nano-$MnFe_2O_4/Al_2O_3$ at different magnification times, the nano-$MnFe_2O_4/Al_2O_3$ adsorbents were successfully synthesized, and the result was in accordance with the following analyses of XRD patterns.

3.1.3. XRD

To further investigate the structure as well as crystallinity before and after modification, the XRD patterns were recorded. The patterns of nano-$MnFe_2O_4$ and nano-$MnFe_2O_4/Al_2O_3$ are described in Fig. 3. The strong diffraction peaks of nano-$MnFe_2O_4$ appeared at 2θ = 30.12°, 35.49°, 42.99°, 57.05° and 62.66°, corresponding to the (220), (311), (400), (511) and (440) planes of $MnFe_2O_4$ according to the Joint Committee on Powder Diffraction card no. 74–2403 [32]. Nevertheless, in the light of the high content of Al_2O_3 when the dipping method was used to synthesize nano-$MnFe_2O_4/Al_2O_3$, the characteristic peaks of nano-$MnFe_2O_4$ either disappeared or the intensity of peaks weakened a large after modification with Al_2O_3. Some new diffraction peaks appeared at 2θ = 36.69°, 46.60° and 68.08°, which could be perfectly assigned to the phase of Al_2O_3 according to JCPDS File NO. 29–63 [20]. Besides, combining the great magnetism observed from the magnetic separation, the conclusion that the magnetic nano-$MnFe_2O_4/Al_2O_3$ adsorbent was successfully synthesized.

3.1.4. Brunauer–Emmett–Teller

The BET technology was used to obtain the specific surface area, pore volume and pore size to predict the adsorption performance. As shown in Fig. 4, the adsorption isotherm of nano-$MnFe_2O_4/Al_2O_3$ was similar to the IV isotherm. In addition, a hysteresis loop similar to H3 type could be observed in the range of 0.2–0.9 relative pressure. This indicated that nano-$MnFe_2O_4/Al_2O_3$ adsorbent mainly comprised from sheet particle or porous material with slit shape. As a matter of fact, a cranny could be found in the SEM image of nano-$MnFe_2O_4/Al_2O_3$ at 20,000 magnification times, which further confirmed the above deductions. The distribution of pore diameter of nano-$MnFe_2O_4/Al_2O_3$ ranged from 2.5 to 40 nm, which indicated that it was mainly an adsorbent based on mesoporous structure. The physical property of synthesized nano-$MnFe_2O_4/Al_2O_3$ was presented in Table 2. The relatively high specific surface

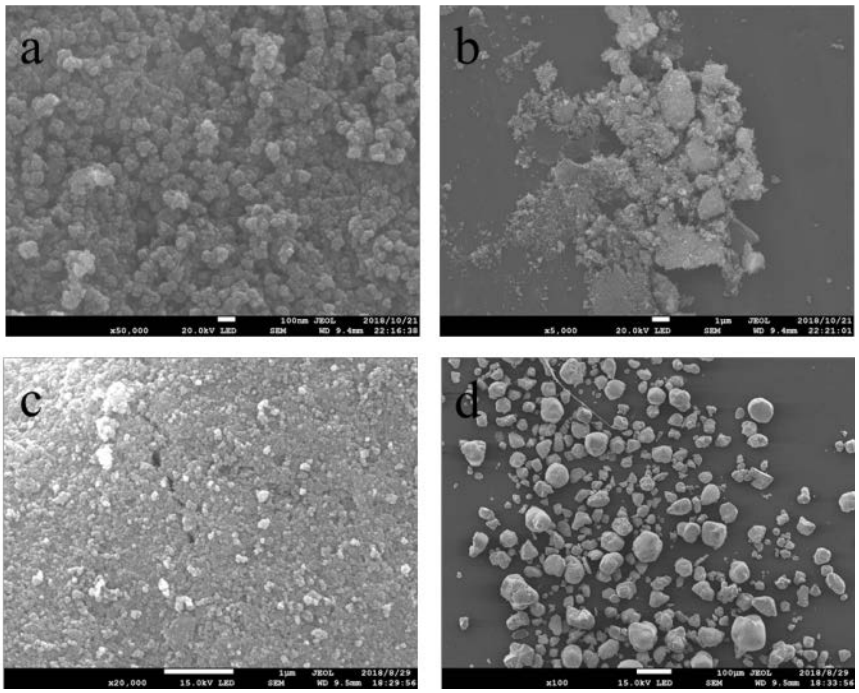

Fig. 2. SEM images of nano-$MnFe_2O_4$ (a: 50,000×, b: 2,000×) and nano-$MnFe_2O_4/Al_2O_3$ (c: 20,000×, d: 100×).

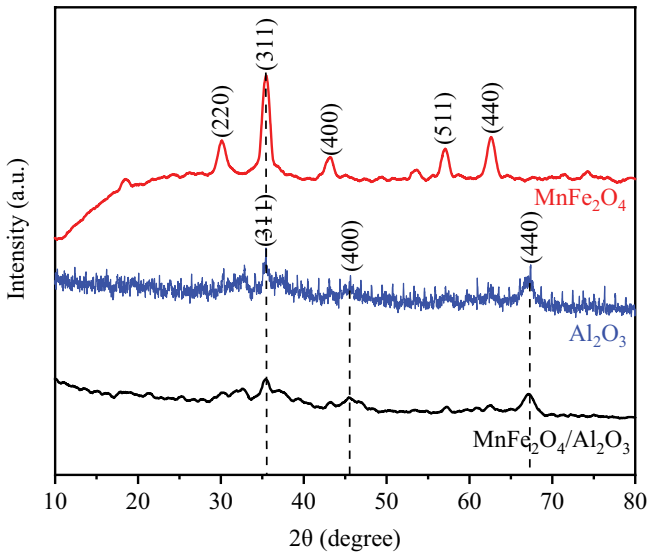

Fig. 3. XRD patterns of nano-$MnFe_2O_4$ and nano-$MnFe_2O_4/Al_2O_3$.

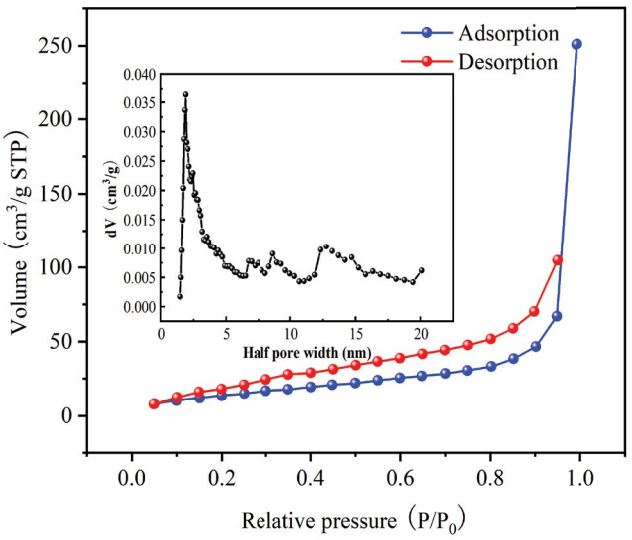

Fig. 4. N_2 adsorption–desorption isotherm and pore size distribution of nano-$MnFe_2O_4/Al_2O_3$.

area (62.79 m^2/g) of nano-$MnFe_2O_4/Al_2O_3$ indicated that it is a promising adsorbent for the Cu^{2+} removal from the aqueous solution.

3.1.5. Fourier transform infrared

The various active functional groups on the surface of the adsorbent play key roles in the adsorption process, which influence the adsorption capacity ultimately [33]. In order to compare the differences of the adsorbents before and after adsorption and further to detect the main functional groups that were responsible for the adsorption process, the FTIR spectrum was measured and depicted in Fig. 5. The broad bands in both spectra appeared at approximately 3,449 and 1,653 cm^{-1}, respectively, which were assigned to stretching vibration and bending vibration of –OH, indicating that there existed hydroxyl groups on the surface of materials [34,35]. In addition, the weak absorption peak at 2,923 cm^{-1} was attributed to the material adsorbing some water molecules in the air during the FTIR analysis, and the other weak peaks at 3,200–3,700 cm^{-1} probably corresponded to the associating hydrogen bond. The absorption peak at 524 and 583 cm^{-1} belong to the characteristic vibration peaks of Metal-O [35], and the absorption peak at 1,023 cm^{-1} before adsorption was attributed to the Metal–OH bond [36].

3.1.6. X-ray photoelectron spectroscopy

With the aid of XPS analysis, not only the elemental composition but also the valence state of the elements on the surface of materials could be understood clearly. Fig. 6 describes

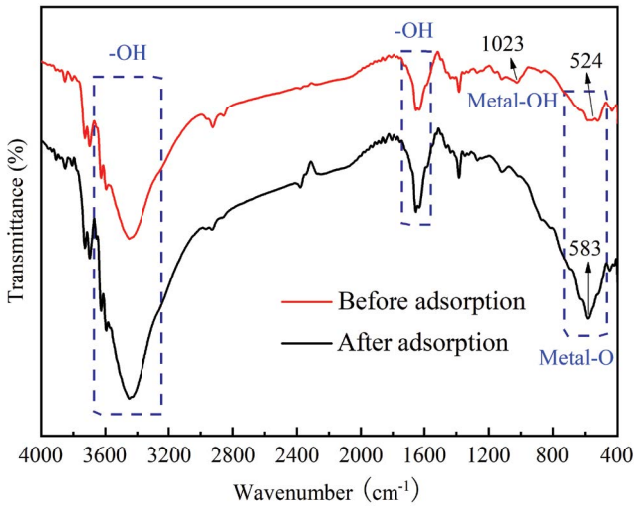

Fig. 5. FTIR spectra of nano-$MnFe_2O_4/Al_2O_3$ before and after adsorption.

the full-survey spectra of nano-$MnFe_2O_4/Al_2O_3$ before and after adsorption. It can be determined well that there were ferrum (Fe), manganese (Mn), aluminum (Al) and oxygen (O) in both samples of nano-$MnFe_2O_4/Al_2O_3$. Owing to the exposure to air and water during sample preparation and reaction, the carbon species could be also observed in both full-survey spectra [37]. Except for C 1s, O 1s, Fe 2p, Mn 2p and Al 2p peaks belonging to nano-$MnFe_2O_4/Al_2O_3$, a

Table 2
Physical property of synthesized $MnFe_2O_4$–Al_2O_3

Adsorbent	BET surface area (m^2/g)	Average pore diameter (nm)	Pore volume (mL/g)
$MnFe_2O_4/Al_2O_3$	62.79	10.2	0.154

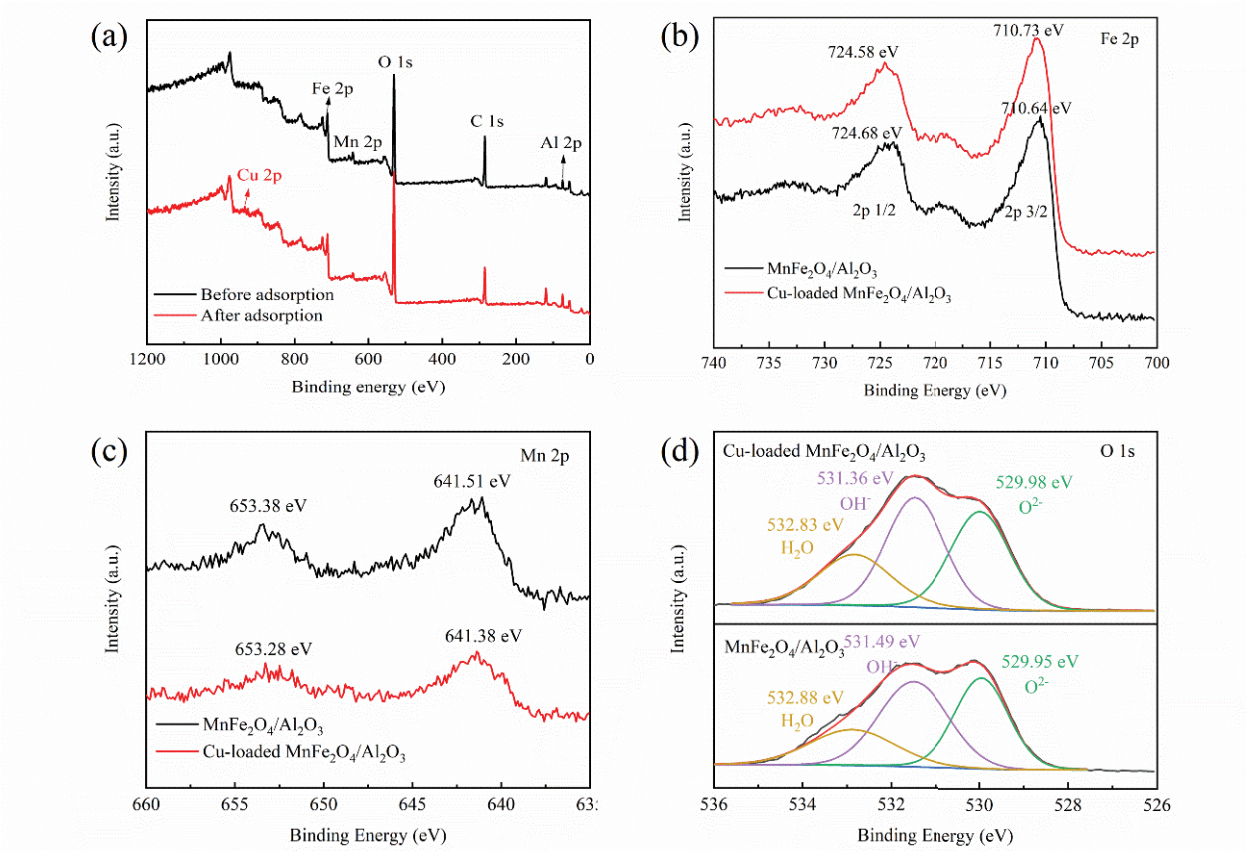

Fig. 6. XPS spectrum of survey (a), Fe 2p (b), Mn 2p (c) and O 1s (d) of nano-$MnFe_2O_4/Al_2O_3$ before and after adsorption.

conspicuous Cu 2p binding energy peak appeared at ca. 930 eV, suggesting that Cu^{2+} ions have been adsorbed onto nano-$MnFe_2O_4/Al_2O_3$ successfully. Figs. 6b–e show the detailed survey of Fe 2p, Mn 2p and O 1s. For Fe 2p region, the photoelectron peaks at 724.58 and 724.68 eV, 710.73 and 710.74 eV were assigned to the binding energies of 2p 1/2 and 2p 3/2, respectively [38]. Moreover, the existence of Fe (III) in the materials could be identified because the separation of spin-orbit energy levels between 2p 1/2 and 2p 3/2 was about 13.9 eV [39]. As to Mn 2p region, the binding energies at 653.38 and 653.28 eV, 641.51 and 641.38 eV were corresponded to 2p 1/2 and 2p 3/2 of Mn [40]. While the presented valence state of Mn 2p 3/2 could not be confirmed, given that the binding energies of Mn^{2+}, Mn^{3+} and Mn^{4+} are extremely close to each other according to XPS electronic binding energy reference table [41]. According to the narrow spectrum of O 1s peak-splitting diagram, the existence of oxygen could be divided into three overlapped peaks, which correspond to oxide oxygen (O^{2-}), hydroxyl groups (OH^-), and adsorbed water (H_2O), respectively [37].

3.2. RSM experimental results and parameter optimization

On the basis of the single factor experiment, according to the design principle of the RSM, the experiment was designed using Design-Expert 10.0 software and Box–Behnken model. According to Box–Behnken design scheme, experiments were carried out to optimize the reaction parameters. The pH (A), the dosage (B), and the reaction time (C) were the main factors to be investigated, and the removal rate was used as the response value (Y) to establish a model and the experimental results are shown in Table S1. According to the experimental results, the regression analysis of the data can obtain the fitting equation:

$$Y = 42.12 + 41.72A + 7.27B + 2.48C + 3.96\,AB + 2.49AC + 0.20BC + 7.54A^2 - 1.55B^2 - 1.07C^2 \quad (7)$$

At the same time, the regression model was analyzed by variance and the results are shown in Table S2. From the analysis of variance of Table S2, the model was highly significant. Among them, the effect of pH was the most significant, and the dosage was second. The misfit term of the model was not significant, and the determination coefficient $R^2 = 0.9984$ indicates that the predicted value and the measured value have a good correlation. In order to consider the influence of various factors and their interaction on adsorption capacity, Design-Expert 10.0 software was used to assist the analysis, and the 3d response surface diagram is shown in Fig. 7. It can be seen from Fig. 7 that pH had the most significant effect on the adsorption capacity, which is consistent with previous related research results. The optimal solution was obtained by Design-Expert 10.0, and the coded value of the stable point corresponding to the maximum value of removal rate (100%) was obtained, which were $A = 1.00$, $B = 0.90$ and $C = 0.00$, respectively. The

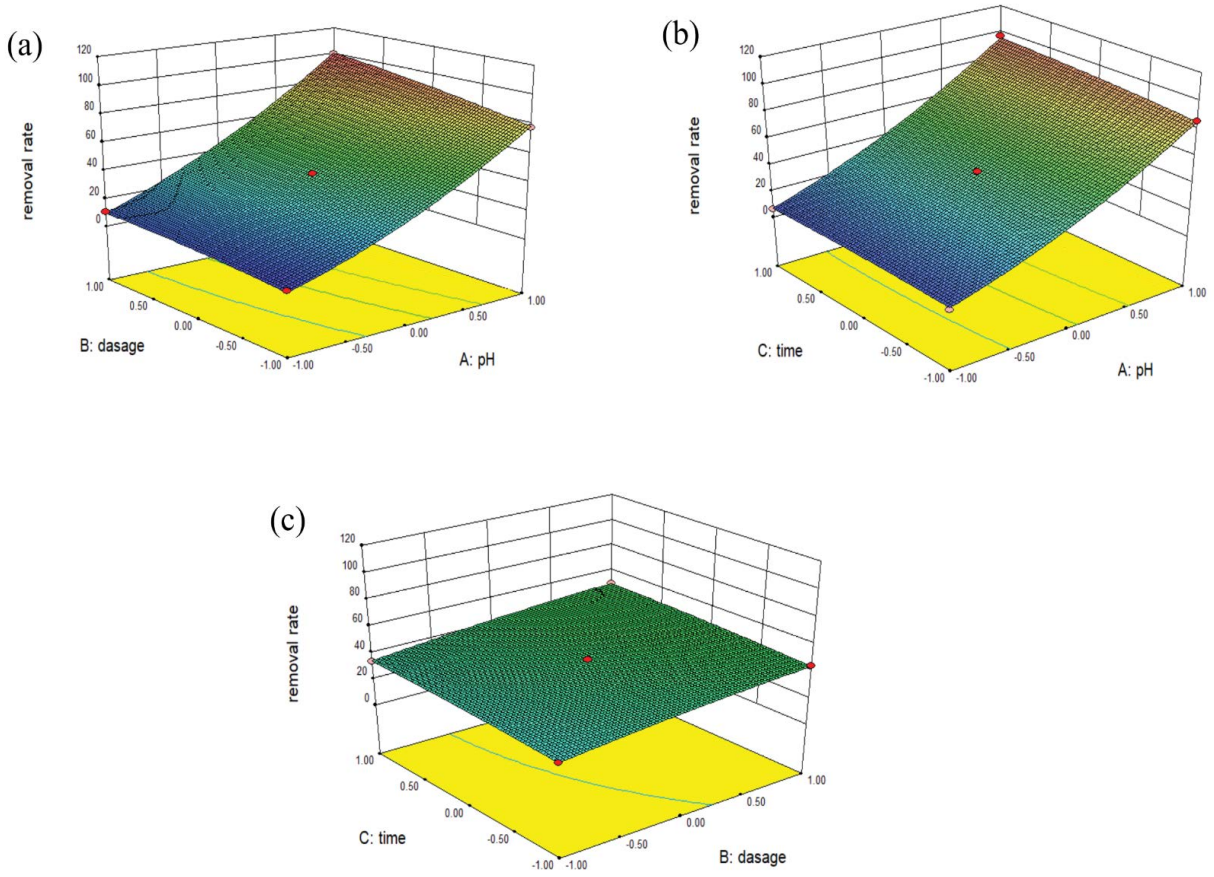

Fig. 7. Response surfaces (3D) showing reciprocal effects of different parameters on adsorption capacity.

corresponding actual values are pH = 6.0, dosage = 0.29 g, reaction time = 3.0 h.

3.3. Adsorption kinetics

The removal efficiencies and adsorption capacities of Cu^{2+} ions vs. contact time onto nano-$MnFe_2O_4/Al_2O_3$ are shown in Fig. 8a. It is evident that the adsorption process of Cu^{2+} ions was divided into three main parts. In the initial stage, the adsorption was carried out extremely rapid. Thereafter, the adsorption slowed down as expressed by the smaller gradient of adsorption curve in the second stage. The reason could be ascribed to the gradual saturation of adsorption sites as contact time was prolonged, which made it difficult for more Cu^{2+} ions to adsorb onto nano-$MnFe_2O_4/Al_2O_3$. The adsorption eventually reached its equilibrium at 180 min with 9.72 mg/g adsorption capacity. The trend of Cu^{2+} removal efficiency was the same as adsorption capacity exhibited. With 180 min adsorption, the removal efficiency of Cu^{2+} reached remarkable 97.2%.

The fitting plots and relevant parameters of pseudo-first-order and pseudo-second-order models are shown in Figs. 8b and c and Table 3, respectively. It can be observed that the correlation coefficient of pseudo-second-order model (R^2 = 0.9986) performed superiority than that of pseudo-first-order model (R^2 = 0.9206), which implied that the adsorption process of Cu^{2+} ions onto nano-$MnFe_2O_4/Al_2O_3$ agree with pseudo-second-order model more preferably. Similar kinetic results were reported for the adsorption kinetics of various water pollutants by organic [42], inorganic [43] and composite [44] adsorbents. As known, the pseudo-first-order model is related to boundary layer. However, this experiment exhibited the insufficient kinetic data, which indicated the adsorption process could be influenced by the limitations of boundary layer [45]. Higher correlation coefficient of pseudo-second-order

Table 3
Kinetic model data for Cu^{2+} adsorption

Pseudo-first-order			Pseudo-second-order		
q_e (mg/g)	k_1 (1/min)	R^2	q_e (mg/g)	k_2 (g/mg min)	R^2
7.37	0.0213	0.9206	10.45	0.0957	0.9986

model suggested that this adsorption process may be based on the rate control step, namely chemical adsorption or electron sharing or exchange between adsorbent and adsorbate [12]. Moreover, the value of adsorption equilibrium concluded from pseudo-second-order model was 10.45 mg/g, which was more close to 9.78 mg/g calculated from the experiment.

3.4. Adsorption isotherms

As illustrated in Fig. 9a, with the increase of Cu^{2+} concentration, the adsorbed amount of Cu^{2+} initially increased quickly, and then tended to be flat. The adsorption capacity of Cu^{2+} onto the adsorbent increased from 2.50 to 14.66 mg/g as the initial Cu^{2+} concentration increased from

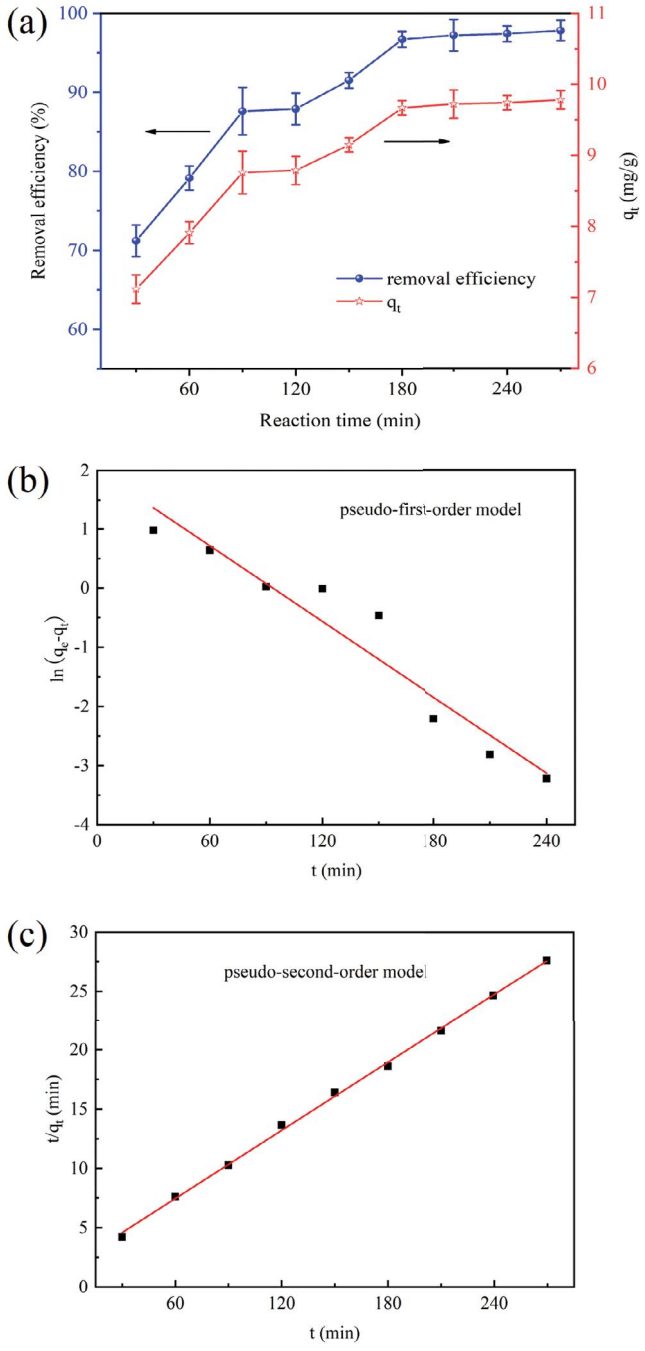

Fig. 8. Effects of contact time on the Cu^{2+} adsorption onto nano-$MnFe_2O_4/Al_2O_3$ (a) and kinetic model fitting plots (b and c) (Cu^{2+} = 20 mg/L; adsorbent dosage = 0.20 g; adsorbate volume = 100 mL; pH = 6.0; temperature = 30°C; shaking speed = 230 rpm).

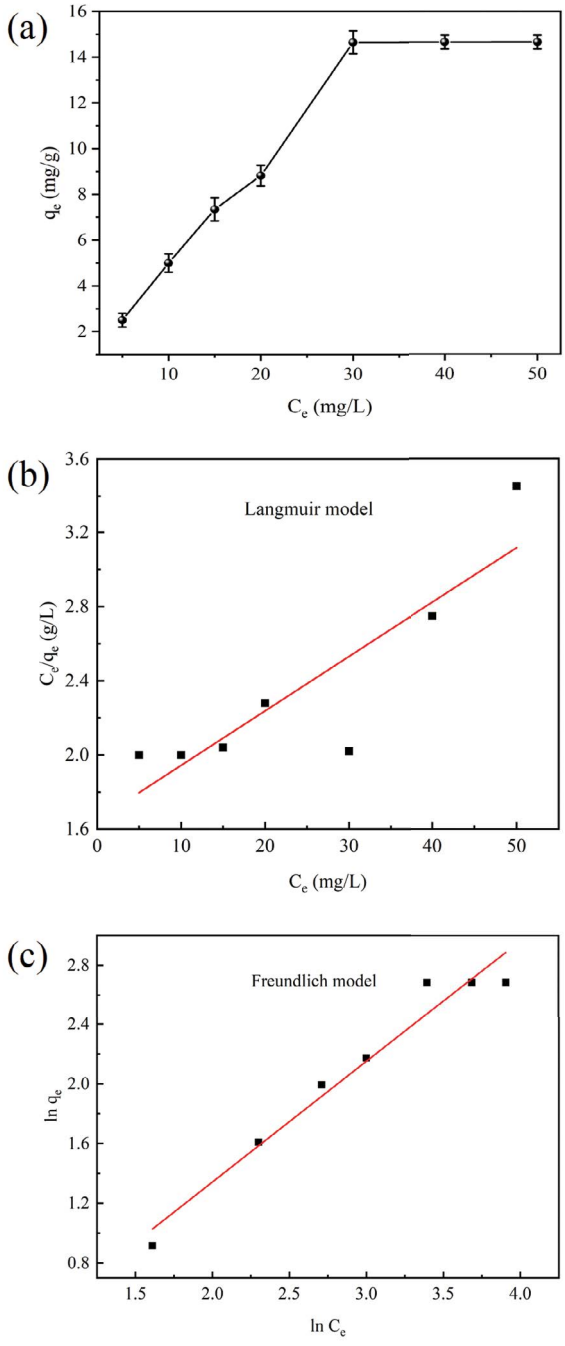

Fig. 9. Effects of Cu^{2+} initial concentration on the Cu^{2+} adsorption onto nano-$MnFe_2O_4/Al_2O_3$ (a) and adsorption isotherm models (b and c) (adsorbent dosage = 0.20 g; adsorbate volume = 100 mL; pH = 6.0; reaction time = 4 h; temperature = 30°C; shaking speed = 230 rpm).

5 to 30 mg/L. However, when the Cu^{2+} concentration was more than 30 mg/L, there was no remarkable increase of adsorption capacity. This indicated that the whole adsorption process achieved adsorption equilibrium at 30 mg/L Cu^{2+} concentration.

On the basis of Langmuir and Freundlich adsorption isotherm models, the parameters of Cu^{2+} adsorption isotherms are described in Table 4. It is apparent that the process of Cu^{2+} adsorption is more satisficing to fit Freundlich adsorption isotherms due to the higher correlation coefficients (R^2 = 0.9531). Whereas the correlation coefficient of Langmuir adsorption isotherms was only 0.7370, it was unsuitable for describing the Cu^{2+} adsorption behavior. Thus, the adsorption of Cu^{2+} onto nano-$MnFe_2O_4/Al_2O_3$ may be an adsorption process of multilayer and heterogeneous surface adsorption [46]. Similar results were obtained for the adsorption isotherms of various adsorbent–adsorbate systems [47,48]. In addition, the value of n was 1.238, which was located in the range of 1–10, indicating the easy conduct of the adsorption.

Table 5 lists the adsorption capacity of several common adsorbents for Cu^{2+}. Through comparison, it can be clearly found that the maximum adsorption capacity of $MnFe_2O_4/Al_2O_3$ prepared in this work is higher than that of most adsorbents, and considering its simple preparation process, low cost and easy enhancement of output, it has a broad practical application.

3.5. Effect of co-existed ions

We know that in the process of industrial production of copper and copper derivatives, there will inevitably be some anions in the discharged wastewater, such as the production of copper sulfate. To confirm the effect of anions on the removal efficiency of Cu^{2+}, the 1.0, 5.0, 20 mg/L concentrations of F^-, Cl^-, NO_3^- and SO_4^{2-} were added into 100 mL of 20 mg/L Cu^{2+} solutions, respectively, and the results are shown in Fig. 10. Moreover, to minimize the error and draw the results accurate as possible, the operating conditions were adopted with the optimal parameters ,which was concluded from the analyses above, that is, pH = 6.0, 0.20 g nano-$MnFe_2O_4/Al_2O_3$, 4 h reaction time, 30°C and 230 rpm. In general, with the addition of anions, the total trend of Cu^{2+} adsorption exhibited downside. However, it is obvious that the existence of given anions at different concentrations has negative effect on the removal of Cu^{2+} ions in the solution. Interestingly, the higher the F^- concentration, the more the Cu^{2+} adsorbed on the nano-$MnFe_2O_4/Al_2O_3$. The reason may be that the increase in F^- concentration strengthened the electrostatic attraction between Cu^{2+} and $MnFe_2O_4/Al_2O_3$ surfaces leading to an increase in the number of collisions between Cu^{2+} and $MnFe_2O_4/Al_2O_3$, thus increasing the removal rate. However, due to the limited adsorption sites of the adsorbent, it can be inferred that the effect of F^- concentration on the removal of Cu^{2+} has not been always a positive relationship when more F^- amount was added. With regard to the critical value, the best F^- concentration that has positive effect should be further investigated.

Table 4
Parameters of Cu^{2+} sorption isotherms using Langmuir and Freundlich models

Langmuir			Freundlich		
q_m (mg/g)	K_L (L/g)	R^2	K_F (mg/g)	n	R^2
34.892	0.0172	0.7370	0.762	1.238	0.9531

3.6. Regeneration and reusability of nano-$MnFe_2O_4/Al_2O_3$

As for an excellent adsorbent, apart from good efficiency towards target pollutant, reusability is another factor which should be taken into consideration for practical application. Based on the magnetism of the adsorbent synthesized that can facilitate its fast separation from aqueous solution with an external magnet added, the study of desorption experiment exhibited great value. Consequently, the five consecutive cycles were carried out, and the results are depicted in Fig. 11. The removal efficiency and adsorption capacity of Cu^{2+} on the nano-$MnFe_2O_4/Al_2O_3$ was 98.2% and 9.82 mg/g, respectively, in its first usage. After five consecutive cycles, the values of removal efficiency and adsorption capacity decreased only a little, but as high as 85.7% and 8.57 mg/g, respectively. These results indicated that the prepared nano-$MnFe_2O_4/Al_2O_3$ has promising application for Cu^{2+} removal in wastewater.

3.7. Adsorption mechanism

By comparing the FTIR spectrum before and after adsorption (Fig. 5), it can be seen clearly that the characteristic absorption peak of Metal-O at 1,023 cm^{-1} almost disappeared after the adsorption of Cu^{2+}, while the characteristic absorption peak at other locations did not change much,

Table 5
Maximum adsorption capacities for the removal of Cu^{2+} by different adsorbents

Adsorbent	Adsorption capacity (mg/g)	References
Oxidized multi-walled carbon nanotubes	29.69	[1]
Brown algae-modified biomass	14.00	[49]
1,4,7-Triazacyclononane modified SBA-15 silica	42.88	[50]
Corncob-derived char wastes	23.58	[51]
Oxide-corncob-derived char wastes	21.88	[51]
$MnFe_2O_4/Al_2O_3$	34.89	This study

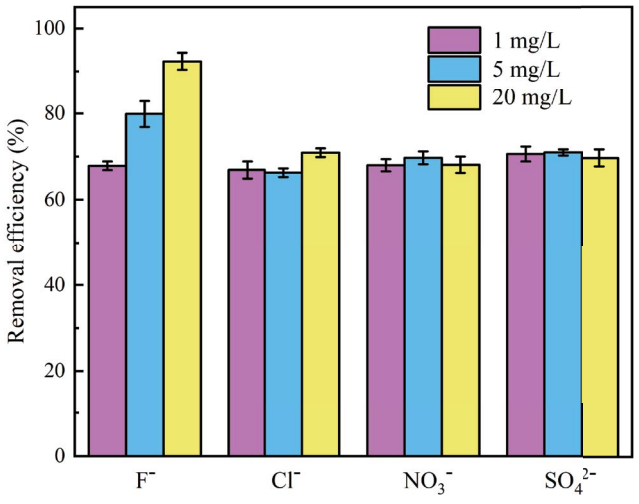

Fig. 10. Effect of F^-, Cl^-, NO_3^- and SO_4^{2-} on the Cu^{2+} adsorption (Cu^{2+} = 20 mg/L, adsorbent dosage = 0.20 g, adsorbate volume = 100 mL, pH = 6.0, temperature = 30°C, shaking speed = 230 rpm).

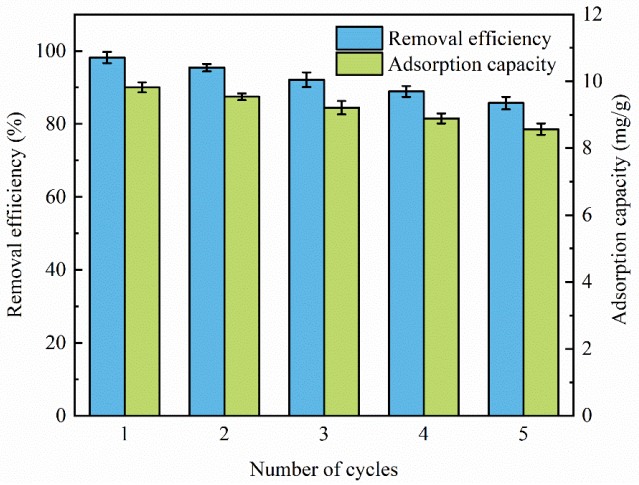

Fig. 11. Effect of cycling times on Cu^{2+} removal efficiency and adsorption capacity (Cu^{2+} = 20 mg/L; adsorbent dosage = 0.20 g; adsorbate volume = 100 mL; pH = 6.0; temperature = 30°C; shaking speed = 230 rpm).

which can be preliminarily inferred that the Metal-O bond played a major role in the adsorption of Cu^{2+}. Moreover, combining with Fig. 6d and Table S3, it can be seen that the binding energy of –OH before and after adsorption deviated from 531.49 to 531.36 eV, which also proves that –OH participated in the reaction. Moreover, as can be observed from Fig. S3, the pH of the solution decreased from 6.0 to 5.6 after adsorption. Hence, it can be said that the adsorption of Cu^{2+} by $MnFe_2O_4/Al_2O_3$ is mainly due to the formation of complex between –OH and Cu^{2+}. The adsorption process is shown in Eq. (8):

$$\frac{2MnFe_2O_4}{Al_2O_3}-OH+Cu^{2+}\rightarrow\left(\frac{MnFe_2O_4}{Al_2O_3-O}\right)_2 Cu+2H^+ \quad (8)$$

4. Conclusions

In this research, a magnetic adsorbent nano-$MnFe_2O_4/Al_2O_3$ was synthesized successfully by coating nano-$MnFe_2O_4$ on the surface of Al_2O_3 via the dipping method and applied for the Cu^{2+} removal from simulated wastewater. The characterizations of VSM, SEM, along with XRD before and after modification illustrated the successful synthesis of magnetic nano-$MnFe_2O_4/Al_2O_3$, while the studies of FTIR and XPS of nano-$MnFe_2O_4/Al_2O_3$ before and after adsorption, as well as adsorption isotherm and kinetics was analyzed for the mechanism of Cu^{2+} adsorption onto nano-$MnFe_2O_4/Al_2O_3$. Moreover, after modification with Al_2O_3, the adsorbents had excellent adsorption property either in the substantial increase of removal efficiency or adsorption capacity. For 100 mL of 20 mg/L Cu^{2+} solution, under the optimal conditions concluded, the removal efficiency of Cu^{2+} reached 100%. The good results of BET parameters and five consecutive cycles also confirmed that the nano-$MnFe_2O_4/Al_2O_3$ was a promising adsorbent and it has the potential to be applied for Cu^{2+} removal in the wastewater.

Supplementary information

Supplementary information includes the effect of pH, the effect of adsorbent dosage, the change of pH value with time, the Box–Behnken experimental design and results and the analysis of Variance (ANOVA).

S1. Effect of pH value

As known, the property of the adsorbent and/or the existence form of heavy metal ions may vary with the change of pH value, and the change would further influence the adsorbate removal efficiency. As shown in Fig. S1a, either $MnFe_2O_4$ or nano-$MnFe_2O_4/Al_2O_3$ as an adsorbent for the Cu^{2+} removal, the tendencies of removal efficiency were in line with the increase of pH value. In the pH range from 1 to 6, the higher the pH value, the more the Cu^{2+} ions adsorbed. As can be seen from Fig. S1b, the pH_{zpc} of $MnFe_2O_4$ and nano-$MnFe_2O_4/Al_2O_3$ were 6.2 and 5.7, respectively. This indicates that when pH = 1.0–5.0, the adsorbents surface carried a large number of positive charges, which generates electrostatic repulsion with Cu^{2+}, leading to a very low removal rate. With the increase of pH, the adsorbents surface carried a negative charge, which generates electrostatic attraction with Cu^{2+}, making the removal rate rise. Nevertheless, at lower pH, a large amount of H^+ appeared in the aqueous solution, which occupied the binding sites that should have been available for Cu^{2+} uptake. At higher pH, OH^- may dominate in the reaction medium and metal ions would have a tendency to get precipitated in the form of metal hydroxides; some of them would escape binding with reaction sites. Hence, when the pH value is greater than 6.0, the removal rate decreased with the increase of pH value. At pH = 6.0, the removal efficiencies and adsorption capacities of Cu^{2+} ions on the two adsorbents reached 50.46% and 74.45%, 10.09 and 14.89 mg/g, respectively.

S2. Effect of adsorbent dosage

Adsorbent dosage is another deciding factor, which has a great effect on both removal efficiency and adsorption

capacity. To find out the best optimal adsorbent dosage and further apply it for subsequent experiments, this part of experiment was carried out. As depicted in Fig. S2, it was observed that the removal efficiencies of Cu^{2+} on both two materials were sharply increased at the initial stage and subsequently tended to be flat with the continuous increase of adsorbent dosage. At 0.05 g adsorbent dosage, the removal efficiencies of Cu^{2+} ions adsorbed on the $MnFe_2O_4$ and

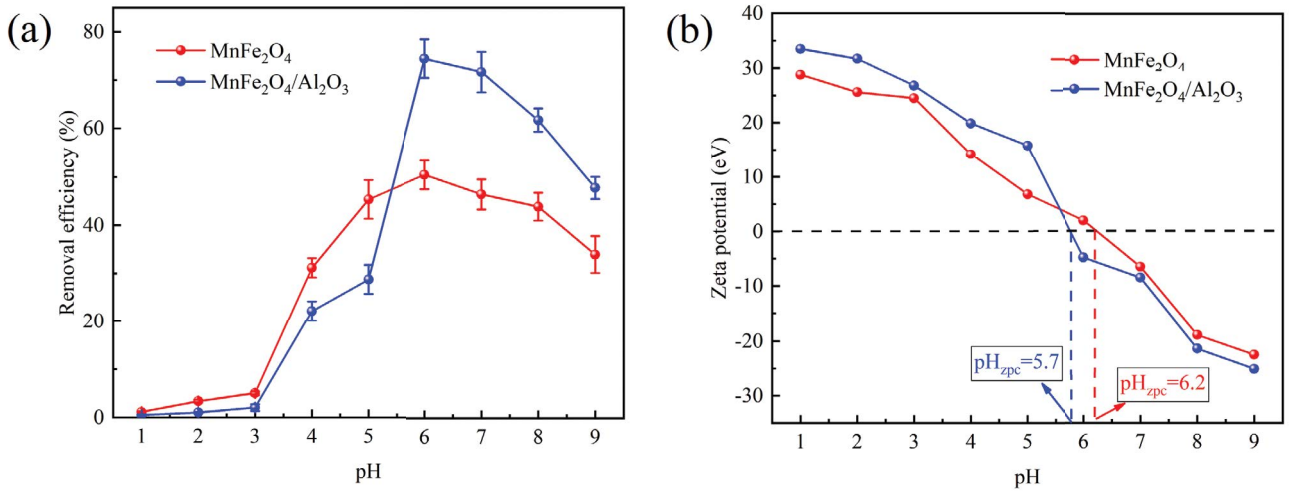

Fig. S1. Effect of initial pH value (a) and the zeta potential of adsorbents (b) (Cu^{2+} = 20 mg/L; adsorbent dosage = 0.10 g; reaction time = 4 h; temperature = 30°C; shaking speed = 230 r/min).

Table S2
Analysis of variance (ANOVA)

Source	Sum of squares	df	Mean square	*F* value	*p*-value	Significance
Model	14,734.13	9	1,637.13	1,104.58	<0.0001	Significant
A-pH	13,926.97	1	13,926.97	9,396.62	<0.0001	
B-dosage	422.97	1	422.97	285.38	<0.0001	
C-time	49.30	1	49.30	33.26	0.0007	
AB	62.65	1	62.65	42.27	0.0003	
AC	24.70	1	24.7	16.67	0.0047	
BC	0.16	1	0.16	0.11	0.7521	
A^2	239.45	1	239.45	161.56	<0.0001	
B^2	10.16	1	10.16	6.86	0.0345	
C^2	4.79	1	4.79	3.23	0.1154	
Residual	10.37	7	1.48			
Lack of fit	10.29	3	3.43	155.86	0.0001	Significant
Pure error	0.088	4	0.022			
Cor total	14,744.51	16				

Table S3
Relative parameters about three overlapped peaks before and after adsorption

Samples	Chemical state	Binding energy (eV)	Percentage (%)
$MnFe_2O_4/Al_2O_3$	O^{2-}	529.95	35.72
	OH^-	531.49	42.03
	H_2O	532.88	22.25
Cu-loaded $MnFe_2O_4/Al_2O_3$	O^{2-}	529.98	35.98
	OH^-	531.46	39.69
	H_2O	532.83	24.33

nano-$MnFe_2O_4/Al_2O_3$ were 38.15% and 61.20%, respectively. As increasing the adsorbent dosage, at 0.20 g $MnFe_2O_4$ and nano-$MnFe_2O_4/Al_2O_3$ dosage, the removal efficiencies of Cu^{2+} ions reached 55.0% and 98.3%, respectively. Afterwards, continuously increasing the adsorbent dosage, the entire adsorption process reached its equilibrium according to that there were almost no change of the removal efficiencies. Thus, 0.20 g $MnFe_2O_4$ and nano-$MnFe_2O_4/Al_2O_3$ dosage were selected to be the best optimal adsorbent dosage for the Cu^{2+} ions adsorption from aqueous solution. It was worth noting that the adsorption capacity was negatively related to the increase of adsorbent dosage. As the $MnFe_2O_4$ and nano-$MnFe_2O_4/Al_2O_3$ increased from 0.05 to 0.20 g, the adsorption capacity of Cu^{2+} ions decreased from 15.26 to 5.50 mg/g and 24.48 to 9.76 mg/g, respectively.

Acknowledgments

This work was supported by the National Natural Sciences Foundation of China (Nos. 51468016 and 51768018), the Natural Sciences Foundation of Jiangxi (No. 20171BAB206047), and the Technology Development Research Project of Jiangxi (No. 200171BBH80008).

References

[1] J. Wang, Z. Li, S. Li, W. Qi, P. Liu, F. Liu, Y. Ye, L. Wu, L. Wang, W. Wu, Adsorption of Cu(II) on oxidized multi-walled carbon nanotubes in the presence of hydroxylated and carboxylated fullerenes, PLoS One, 8 (2013) e72475.
[2] Y. Xie, X. Yuan, Z. Wu, G. Zeng, L. Jiang, X. Peng, H. Li, Adsorption behavior and mechanism of Mg/Fe layered double hydroxide with Fe_3O_4-carbon spheres on the removal of Pb(II) and Cu(II), J. Colloid Interface Sci., 536 (2019) 440–455.
[3] E. Ayranci, O. Duman, Removal of anionic surfactants from aqueous solutions by adsorption onto high area activated carbon cloth studied by in situ UV spectroscopy, J. Hazard. Mater., 148 (2007) 75–82.
[4] E. Ayranci, O. Duman, Adsorption behaviors of some phenolic compounds onto high specific area activated carbon cloth, J. Hazard. Mater., 124 (2005) 125–132.
[5] O. Duman, E. Ayranci, Structural and ionization effects on the adsorption behaviors of some anilinic compounds from aqueous solution onto high-area carbon-cloth, J. Hazard. Mater., 120 (2005) 173–181.
[6] X. Song, L. Li, L. Zhou, P. Chen, Magnetic thiolated/quaternized-chitosan composites design and application for various heavy metal ions removal, including cation and anion, Chem. Eng. Res. Design, 136 (2018) 581–592.
[7] A. Denizli, G. Özkan, M.Y. Arica, Preparation and characterization of magnetic polymethylmethacrylate microbeads carrying ethylene diamine for removal of Cu(II), Cd(II), Pb(II), and Hg(II) from aqueous solutions, J. Appl. Polym. Sci., 78 (2015) 81–89.
[8] Y. Yong, T. Yonezawa, M. Matsubara, H. Tsukamoto, The mechanism of alkylamine-stabilized copper fine particles towards improving the electrical conductivity of copper films at low sintering temperature, J. Mater. Chem. C, 3 (2015) 5890–5895.
[9] M.R. Awual, M.M. Hasan, Colorimetric detection and removal of copper(II) ions from wastewater samples using tailor-made composite adsorbent, Sens. Actuat. B: Chem., 206 (2015) 692–700.
[10] Z. Liu, X. Li, P. Zhan, F. Hu, X. Ye, Removal of cadmium and copper from water by a magnetic adsorbent of PFM: adsorption performance and micro-structural morphology, Sep. Purif. Technol., 206 (2018) 199–207.
[11] S.Y. Choi, V.T. Nguyen, J.C. Lee, H. Kang, B.D. Pandey, Liquid-liquid extraction of Cd(II) from pure and Ni/Cd acidic chloride media using Cyanex 921: a selective treatment of hazardous leachate of spent Ni-Cd batteries, J. Hazard. Mater., 278 (2014) 258–266.
[12] H. Liu, Y. Dong, H. Wang, Y. Liu, Ammonium adsorption from aqueous solutions by strawberry leaf powder: equilibrium, kinetics and effects of coexisting ions, Desalination, 263 (2010) 70–75.
[13] S. Golbaz, A.J. Jafari, M. Rafiee, R.R. Kalantary, Separate and simultaneous removal of phenol, chromium, and cyanide from aqueous solution by coagulation/precipitation: mechanisms and theory, Chem. Eng. J., 253 (2014) 251–257.
[14] S. Logette, C. Eysseric, G. Pourcelly, A. Lindheimer, C. Gavach, Selective permeability of a perfluorosulphonic membrane to different valency cations. Ion-exchange isotherms and kinetic aspects, J. Membr. Sci., 144 (1998) 259–274.
[15] M. Cataldo Hernández, L. Barletta, M.B. Dogliotti, N. Russo, D. Fino, P. Spinelli, Heavy metal removal by means of electrocoagulation using aluminum electrodes for drinking water purification, J. Appl. Electrochem., 42 (2012) 809–817.
[16] F. Quartinello, S. Vajnhandl, J. Volmajer Valh, T.J. Farmer, B. Voncina, A. Lobnik, E. Herrero Acero, A. Pellis, G.M. Guebitz, Synergistic chemo-enzymatic hydrolysis of poly(ethylene terephthalate) from textile waste, Microb. Biotechnol., 10 (2017) 1376–1383.
[17] S. Duan, X. Xu, X. Liu, Y. Wang, T. Hayat, A. Alsaedi, Y. Meng, J. Li, Highly enhanced adsorption performance of U(VI) by non-thermal plasma modified magnetic Fe_3O_4 nanoparticles, J. Colloid Interface Sci., 513 (2018) 92–103.
[18] N. Sezgin, A. Yalçın, Y. Köseoğlu, $MnFe_2O_4$ nano spinels as potential sorbent for adsorption of chromium from industrial wastewater, Desal. Water Treat., 57 (2015) 16495–16506.
[19] T.A. Saleh, A. Sarı, M. Tuzen, Effective adsorption of antimony(III) from aqueous solutions by polyamide-graphene composite as a novel adsorbent, Chem. Eng. J., 307 (2017) 230–238.
[20] S. Banerjee, R.K. Gautam, A. Jaiswal, M. Chandra Chattopadhyaya, Y. Chandra Sharma, Rapid scavenging of methylene blue dye from a liquid phase by adsorption on alumina nanoparticles, RSC Adv., 5 (2015) 14425–14440.
[21] G. Patra, P. Das, S. Chakraborty, B.C. Meikap, Removal of fluoride from wastewater using HCl-treated activated alumina in a ribbed hydrocyclone separator, J. Environ. Sci. Health, Part A Toxic Hazard. Subst. Environ. Eng., 53 (2018) 601–608.
[22] A. Rahmani, H.Z. Mousavi, M. Fazli, Effect of nanostructure alumina on adsorption of heavy metals, Desalination, 253 (2010) 94–100.
[23] H. Wei, S. Deng, Q. Huang, Y. Nie, B. Wang, J. Huang, G. Yu, Regenerable granular carbon nanotubes/alumina hybrid adsorbents for diclofenac sodium and carbamazepine removal from aqueous solution, Water Res., 47 (2013) 4139–4147.
[24] L. Sun, X. Sun, X. Du, Y. Yue, L. Chen, H. Xu, Q. Zeng, H. Wang, L. Ding, Determination of sulfonamides in soil samples based on alumina-coated magnetite nanoparticles as adsorbents, Anal. Chim. Acta, 665 (2010) 185–192.
[25] N.A. Bahari, W.N.R.W. Isahak, M.S. Masdar, M.M. Ba-Abbad, Optimization of the controllable crystal size of iron/zeolite nanocomposites using a Box–Behnken design and their catalytic activity, Appl. Nanosci., 9 (2018) 209–224.
[26] E. Alver, A.Ü. Metin, Anionic dye removal from aqueous solutions using modified zeolite: adsorption kinetics and isotherm studies, Chem. Eng. J., 200–202 (2012) 59–67.
[27] Z. Zou, Z. Shi, L. Deng, Highly efficient removal of Cu(II) from aqueous solution using a novel magnetic EDTA functionalized $CoFe_2O_4$, RSC Adv., 7 (2017) 5195–5205.
[28] S. Vafakhah, M.E. Bahrololoom, R. Bazarganlari, M. Saeedikhani, Removal of copper ions from electroplating effluent solutions with native corn cob and corn stalk and chemically modified corn stalk, J. Environ. Chem. Eng., 2 (2014) 356–361.
[29] Z. Liu, G. Chen, F. Hu, X. Li, Synthesis of mesoporous magnetic $MnFe_2O_4$@CS-SiO_2 microsphere and its adsorption performance

of $Zn^{(2+)}$ and MB studies, J. Environ. Manage., 263 (2020) 110377.
[30] J. Chen, W. Zhang, X. Li, Adsorption of Cu(II) ion from aqueous solutions on hydrogel prepared from Konjac glucomannan, Polym. Bull., 73 (2015) 1965–1984.
[31] C. Amorim, G. Yuan, P. Patterson, M. Keane, Catalytic hydrodechlorination over Pd supported on amorphous and structured carbon, J. Catal., 234 (2005) 268–281.
[32] Y. Wang, X. Wu, W. Zhang, S. Huang, One-pot synthesis of $MnFe_2O_4$ nanoparticles-decorated reduced graphene oxide for enhanced microwave absorption properties, Mater. Technol., 32 (2016) 32–37.
[33] S. Ghysels, F. Ronsse, Comment on "Redox-Active Oxygen-containing functional groups in activated carbon facilitate microbial reduction of ferrihydrite", Environ. Sci. Technol., 52 (2018) 4485–4486.
[34] S. Lan, N. Guo, L. Liu, X. Wu, L. Li, S. Gan, Facile preparation of hierarchical hollow structure gamma alumina and a study of its adsorption capacity, Appl. Surf. Sci., 283 (2013) 1032–1040.
[35] J. Liang, J. Liu, X. Yuan, H. Dong, G. Zeng, H. Wu, H. Wang, J. Liu, S. Hua, S. Zhang, Z. Yu, X. He, Y. He, Facile synthesis of alumina-decorated multi-walled carbon nanotubes for simultaneous adsorption of cadmium ion and trichloroethylene, Chem. Eng. J., 273 (2015) 101–110.
[36] Z. Cheng, F. Fu, D.D. Dionysiou, B. Tang, Adsorption, oxidation, and reduction behavior of arsenic in the removal of aqueous As(III) by mesoporous Fe/Al bimetallic particles, Water Res., 96 (2016) 22–31.
[37] Z. Wen, Y. Zhang, C. Dai, B. Chen, S. Guo, H. Yu, D. Wu, Synthesis of ordered mesoporous iron manganese bimetal oxides for arsenic removal from aqueous solutions, Microporous Mesoporous Mater., 200 (2014) 235–244.
[38] D. Wilson, M.A. Langell, XPS analysis of oleylamine/oleic acid capped Fe_3O_4 nanoparticles as a function of temperature, Appl. Surf. Sci., 303 (2014) 6–13.
[39] T. Yamashita, P. Hayes, Analysis of XPS spectra of Fe^{2+} and Fe^{3+} ions in oxide materials, Appl. Surf. Sci., 254 (2008) 2441–2449.
[40] J. Liu, M.P. Hanson, J.A. Peters, B.W. Wessels, Magnetism and Mn Clustering in (In,Mn)Sb Magnetic Semiconductors, ACS Appl. Mater. Interfaces, 7 (2015) 24159–24167.
[41] R. Guillet-Nicolas, M. Laprise-Pelletier, M.M. Nair, P. Chevallier, J. Lagueux, Y. Gossuin, S. Laurent, F. Kleitz, M.A. Fortin, Manganese-impregnated mesoporous silica nanoparticles for signal enhancement in MRI cell labelling studies, Nanoscale, 5 (2013) 11499–11511.
[42] E. Ayranci, O. Duman, Structural effects on the interactions of benzene and naphthalene sulfonates with activated carbon cloth during adsorption from aqueous solutions, Chem. Eng. J., 156 (2010) 70–76.
[43] O. Duman, S. Tunç, T.G. Polat, Determination of adsorptive properties of expanded vermiculite for the removal of C. I. Basic Red 9 from aqueous solution: kinetic, isotherm and thermodynamic studies, Appl. Clay Sci., 109–110 (2015) 22–32.
[44] O. Duman, C. Özcan, T. Gürkan Polat, S. Tunç, Carbon nanotube-based magnetic and non-magnetic adsorbents for the high-efficiency removal of diquat dibromide herbicide from water: OMWCNT, OMWCNT-Fe_3O_4 and OMWCNT-κ-carrageenan-Fe_3O_4 nanocomposites, Environ. Pollut., 244 (2019) 723–732.
[45] P.P. Remy, M. Etique, A.A. Hazotte, A.S. Sergent, N. Estrade, C. Cloquet, K. Hanna, F.P. Jorand, Pseudo-first-order reaction of chemically and biologically formed green rusts with HgII and $C_{15}H_{15}N_3O_2$: effects of pH and stabilizing agents (phosphate, silicate, polyacrylic acid, and bacterial cells), Water Res., 70 (2015) 266–278.
[46] O. Tunc, H. Tanaci, Z. Aksu, Potential use of cotton plant wastes for the removal of Remazol Black B reactive dye, J. Hazard. Mater., 163 (2009) 187–198.
[47] O. Duman, E. Ayranci, Attachment of benzo-crown ethers onto activated carbon cloth to enhance the removal of chromium, cobalt and nickel ions from aqueous solutions by adsorption, J. Hazard. Mater., 176 (2010) 231–238.
[48] E. Ayranci, O. Duman, Adsorption of aromatic organic acids onto high area activated carbon cloth in relation to wastewater purification, J. Hazard. Mater., 136 (2006) 542–552.
[49] R. Foroutan, H. Esmaeili, M. Abbasi, M. Rezakazemi, M. Mesbah, Adsorption behavior of Cu(II) and Co(II) using chemically modified marine algae, Environ. Technol., 39 (2018) 2792–2800.
[50] P.K. Tapaswi, M.S. Moorthy, S.S. Park, C.-S. Ha, Fast, selective adsorption of Cu^{2+} from aqueous mixed metal ions solution using 1,4,7-triazacyclononane modified SBA-15 silica adsorbent (SBA-TACN), J. Solid State Chem., 211 (2014) 191–199.
[51] X.X. Hou, Q.F. Deng, T.Z. Ren, Z.Y. Yuan, Adsorption of $Cu^{(2+)}$ and methyl orange from aqueous solutions by activated carbons of corncob-derived char wastes, Environ. Sci. Pollut. Res. Int., 20 (2013) 8521–8534.